Self-Assembled Hyperbranched Polymer-Gold Nanoparticle Hybrids: Understanding the Effect of Polymer Coverage on Assembly Size and SERS Performance

ARTICLE *in* LANGMUIR · DECEMBER 2012

Impact Factor: 4.46 · DOI: 10.1021/la304034b · Source: PubMed

4 AUTHORS, INCLUDING:

Priyanka Dey
Ludwig-Maximilians-University of Munich
7 PUBLICATIONS **45** CITATIONS

SEE PROFILE

Idriss Blakey
University of Queensland
98 PUBLICATIONS **882** CITATIONS

SEE PROFILE

Kristofer J. Thurecht
University of Queensland
86 PUBLICATIONS **1,281** CITATIONS

SEE PROFILE

Langmuir

Article

pubs.acs.org/Langmuir

Self-Assembled Hyperbranched Polymer–Gold Nanoparticle Hybrids: Understanding the Effect of Polymer Coverage on Assembly Size and SERS Performance

Priyanka Dey,[†] Idriss Blakey,[‡] Kristofer J. Thurecht,[‡] and Peter M. Fredericks*[,†]

[†]School of Chemistry, Physics and Mechanical Engineering, Queensland University of Technology, Brisbane, Queensland 4001, Australia

[‡]Australian Institute of Bioengineering and Nanotechnology and Centre for Advanced Imaging, University of Queensland, St. Lucia, Queensland 4072, Australia

Supporting Information

ABSTRACT: In the past few years, remarkable progress has been made in unveiling novel and unique optical properties of strongly coupled plasmonic nanostructures. However, the application of such plasmonic nanostructures in biomedicine remains challenging because of the lack of facile and robust assembly methods for producing stable nanostructures. Previous attempts to achieve plasmonic nanoassemblies using molecular ligands were limited by the lack of flexibility that could be exercised in forming them. Here, we report the utilization of tailor-made hyperbranched polymers (HBP) as linkers to assemble gold nanoparticles (NPs) into nano-assemblies. The ease and flexibility in tuning the particle size and number of branch ends of an HBP make it an ideal candidate as a linker, as opposed to DNA, small organic molecules, and linear or dendrimeric polymers. We report a strong correlation of polymer (HBP) concentration with the size of the hybrid nanoassemblies and "hot-spot" density. We have shown that such solutions of stable HBP–gold nanoassemblies can be barcoded with various Raman tags to provide improved surface-enhanced Raman scattering (SERS) compared to that of nonaggregated NP systems. These Raman-barcoded hybrid nanoassemblies, with further optimization of the NP shape, size, and hot-spot density, may find application as diagnostic tools in nanomedicine.

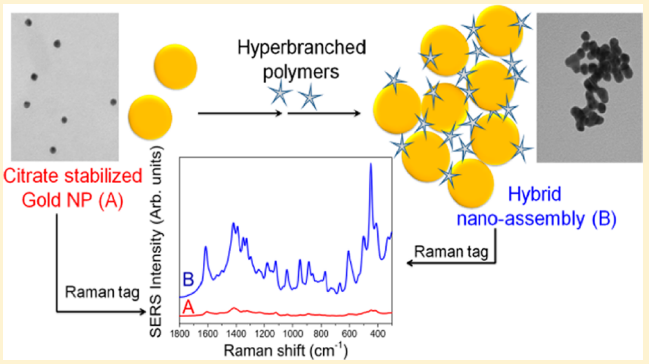

INTRODUCTION

Successful efforts during the past decade have resulted in novel colloid chemistry methods for the controlled assembly of plasmonic nanoparticles (NPs). Noble metal NPs are excellent candidates for plasmonic building blocks because of both their chemical inertness and their ability to support localized surface plasmon resonances (LSPRs) in the visible to near-infrared (NIR) regions. When plasmonic NPs are close to each other, individual plasmon oscillations can couple via near-field interactions, resulting in coupled LSPR modes,[1,2] which strongly impacts the distribution of the electric field around the nanostructure.[3] A number of recent studies have demonstrated applications based on the use of plasmonic NPs, including catalysis,[4] imaging, and detection of either biologically[5−8] or environmentally relevant analytes.[9,10]

When Raman-active molecules are adsorbed in the interstitial gaps between nanoparticles (NPs) within NP assemblies (often referred to as "hot spots"), their Raman signals are dramatically enhanced, a phenomenon known as surface-enhanced Raman scattering (SERS).[11−14] Thus, one of the major areas of research comprising NP assemblies focuses on the development of barcoded NPs for biodetection and labeling with SERS.[15−17] Advanced sensor devices based on barcoded NPs would be capable of monitoring multiple parameters in a complex mixture along with the possibility of selectively imaging parts of the organs, tissues, and cells within living organisms.[18] Major requirements for these barcoded NPs include hot-spot activity and size. A high hot-spot density allows efficient NP identification through SERS, thus avoiding structural damage to biomolecules, which is essential when the NPs are used for imaging in living organisms (tissues or cells). Size is another key parameter, especially when dealing with the migration of NPs into the cells via the enhanced permeability and retention (EPR) effect.[19,20] Liz-Marzán and co-workers[21] in a recent review have pointed out that the available Raman-barcoded assemblies are usually large and their size either completely inhibits migration into the cell or results in the inclusion of only a very small number of "big particles", dramatically decreasing

Received: October 11, 2012
Revised: December 14, 2012
Published: December 17, 2012

Scheme 1. Polymer Structure, Synthesis and Hybrid Nanoassembly[a]

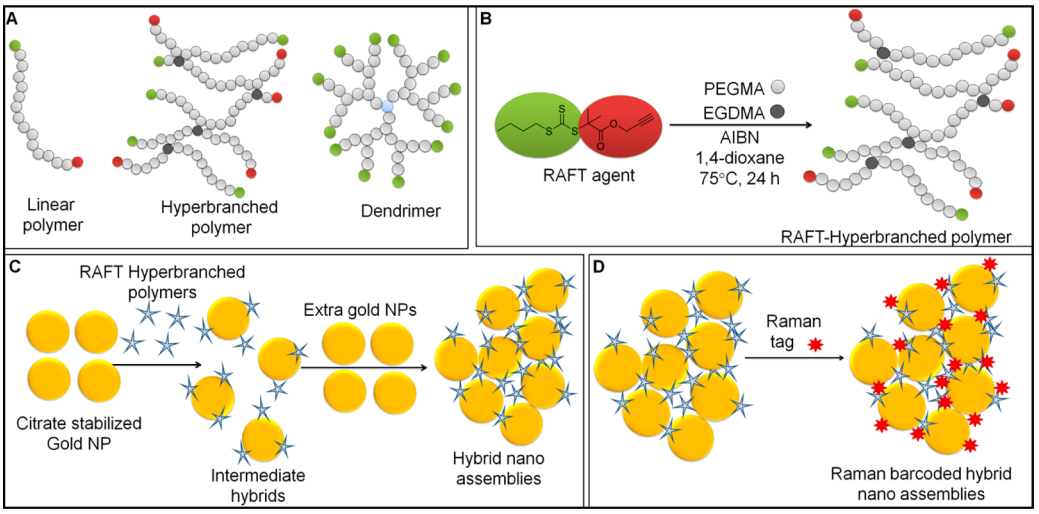

[a](A) Structural differences among linear, hyperbranched, and dendritic polymers. (B) Synthesis scheme of hyperbranched polymers using the reversible addition−fragmentation chain-transfer (RAFT) polymerization technique. (C) Scheme for the formation of hybrid HBP−gold nanoassemblies. (D) Scheme for barcoding the hybrid nanoassemblies with a Raman tag molecule.

the spatial resolution for imaging purposes. Thus, there is a scope for the development of plasmonic assemblies of a suitable size range and SERS activity for applications in biodiagnostics.

Three main approaches to direct the assembly of discrete NPs can be summarized as (i) the asymmetric functionalization of the linkers to the NP building blocks, (ii) control of the aggregation kinetics by destabilizing the electrostatic interactions of a colloidal system, and (iii) the use of molecular linkers. Among them, the most promising and versatile approach is the use of molecular linkers, which allows the possibility to tailor the assembly size, hot-spot density, and interparticle distance. Researchers have utilized various molecular ligands including DNA, small organic ligands, and polymeric ligands as linkers to self-assemble gold NPs. Although DNA[22−24] has the ability to control the assembly precisely, it lacks structural rigidity and bending properties and thus it has been challenging to use it as a versatile linker. Tailor-made organic and polymeric ligands with functional groups known to interact with gold surfaces include thiols,[25] disulfides,[26] isothiocyanates,[27] terminal acetylenes,[28−30] diisocyanides,[31] iodoperfluorobenzenes,[32] trithiocarbonates,[33] and dithioesters.[33,34] The self-assembly of monofunctional polymers or small molecules around gold NPs has been achieved using a number of these functionalities, which typically results in stabilized single NPs.[35−38] However, when polyvalent polymers or small molecules are used, they can direct the self-assembly of gold NPs. For example, efforts have been reported, where alkanethiols,[25] siloxanes,[39] aminosilane,[40] and cucurbit[5]uril[41] have been successfully employed as linkers. Polavarapu et al.[42] employed a cationic polymer to induce solution-phase aggregation by adjusting the polymer-to-gold NP ratio. The formed gold nanochains acted as a SERS substrate, attaining an enhancement factor (EF) of ∼8.4 × 10^9 with Rhodamine 6G. Rotello and co-workers[43,44] have shown that gold NP assemblies can be systematically constructed by a "bricks and mortar" approach, where recognition-element-functionalized gold NPs act as the bricks and polymers bearing complementary functionality serve as the mortar. They have successfully demonstrated that poly(amidoamine) (PAMAM) dendrimers can be employed to self-assemble gold NPs via electrostatic interactions, resulting in a film with an interparticle spacing of ∼2.1 nm. Pan et al.[45] have shown similar behavior for gold NP assemblies utilizing thiol-terminated dendrimers. In particular, Zhong and co-workers[46,47] have demonstrated an elegant approach in a series of publications showing that spherical assemblies of gold NPs can be prepared from solution by using specifically designed tridentate and tetradentate thioethers as mediators in the presence of tetraalkyl ammonium bromide. They have shown that the interparticle spacing and structures of the nanoparticle assemblies can be manipulated by the different shapes (I, V, X, Y) of the rigid methylthio arylethynes (MTA). Depending on the number of interacting thio groups (which varied with the shape), they achieved an assembly size in the range of 50−500 nm and SERS EF values of (1−6) × 10^4 with the MTAs comprising the hot spots.[47] Such solutions of stable assemblies are an appealing prospect for developing active Raman-barcoded assemblies for application in biodiagnostics. There has been some investigation and success in forming gold NP assemblies by utilizing multibranched structures such as multidentate small molecular ligands and dendrimers. However, the preparation of these multidentate structures involves multistep syntheses and purification processes as well as complex procedures to incorporate more branches. In contrast, the synthesis of multibranched structures such as hyperbranched polymers (HBP) involves a one-step synthesis and purification process. Their synthesis mechanism allows the flexibility to introduce and control the number of branches in a one-pot method. HBPs also find application in biomedical settings, which has been widely demonstrated in the literature.[48,49]

In this work, we introduce a new preparative rationale for hybrid gold nanoassemblies and demonstrate that HBPs can be employed to direct the self-assembly of gold NPs. Such Raman-barcoded assemblies may have the potential for bioconjugation and drug incorporation via the functional end groups of the HBPs. HBPs with functional end groups that have an affinity for gold surfaces (i.e., trithiocarbonate or dithioester end groups[33]) can be readily synthesized by reversible addition−fragmentation chain-transfer (RAFT) polymerization.[50] Hence, RAFT-synthesized HBP presents itself as a potential linker for

dx.doi.org/10.1021/la304034b | *Langmuir* 2013, 29, 525−533

the directed assembly of gold NPs. Here, we investigate the parameters that affect the self-assembly of gold NPs mediated by HBPs and their application as Raman-barcoded assemblies.

EXPERIMENTAL SECTION

Materials. Prior to use, poly(ethyleneglycol) monomethylether methacrylate (PEGMA-475), ethylene glycol dimethylacrylate (EGDMA), and 1,4-dioxane were purified by passage through a column of basic alumina. Azobisisobutyronitrile (AIBN) was recrystallized from methanol. All of the above were obtained from Sigma-Aldrich. Tetrachloroauric acid and trisodium citrate were obtained from PST and used as received. Methylene blue, adenine, indocyanine green, and 2-quinolinethiol were obtained from Sigma-Aldrich. Deuterated chloroform ($CDCl_3$) from Sigma-Aldrich was used as the NMR solvent, and tetrahydrofuran (THF) was used as the GPC solvent. Ultrapure water (18 MΩ) was used in all experiments.

Synthesis of Citrate-Stabilized Gold NPs. Gold NPs were synthesized by a slight variation of the Frens[51] and Turkevich[52] method. A $HAuCl_4 \cdot 3H_2O$ solution (0.3 mM, 100 mL) was brought to boiling. A trisodium citrate solution (1 wt %, 4.3 mL) was added, after which the solution started to turn purplish and finally red. The reaction was refluxed for 10 min. A 2 nM gold colloid was thus obtained with λ_{SPR} at 519 nm, a TEM median diameter of 17 ± 1 nm, and a DLS mean diameter of 18 ± 3 nm.

Synthesis of RAFT Hyperbranched Polymers (HBP). The RAFT agent was synthesized in two steps: first the carboxyl derivative was synthesized following a literature method,[53] and then it was converted to its alkyne derivative by reacting it with propagyl alcohol. The product was characterized by ^{1}H NMR, and the alkyne derivative was used as the RAFT agent in the polymerization. HBPs were prepared by polymerizing poly(ethylene glycol) monomethylether methacrylate (PEGMA) (monomer) with ethylene glycol dimethacrylate (EGDMA) (branching agent), which was initiated by azobisisobutyronitrile (AIBN) in the presence of dimethyl(prop-2-ynyl propanoate)yl butyl trithiocarbonate as the RAFT, where dioxane was used as a solvent (Scheme 1B). The reaction mixture was degassed with argon, and the polymerization was carried out at 75 °C for 24 h. A ratio of 20/1/1/0.1 [M]/[RAFT]/[EGDMA]/[AIBN] was employed. The polymerization reached 96% conversion as determined by Raman spectroscopy, where the consumption of the double bonds during the reaction was monitored. The polymer was then precipitated in *n*-hexane, and its aqueous solution was dialyzed for 5 days against water. The dialyzed samples were freeze-dried for 2 days. They were passed over magnesium sulfate and finally left overnight in a vacuum oven to remove the last traces of water. The samples were analyzed by ^{1}H NMR and GPC-MALLS. The M_n of the branch was calculated by the ratio of the number of methylene groups of p(PEGMA) to the number of methylene groups adjacent to the terminal alkyne end group (i.e., ratio of peak integrals at 4.0 ppm (CH_2CH_2O) to those at 4.6 ppm (CH_2CCH) from ^{1}H NMR). Thus, we calculated the number of branches from the ratio of the GPC-MALLS M_n to the M_n of a branch from NMR using detailed calculations reported by Thurecht and co-workers.[49,50]

Preparation of Hybrid HBP Gold Nanoassemblies. The HBP stock solution (0.1−100 μM, 50 μL) was added to 3 mL of 2 nM citrate-stabilized gold NPs and vortex mixed for 2 to 3 min. The colloid, which was still red, was left standing overnight to form an intermediate hybrid of gold NPs coated with varying degrees of HBP. It was hypothesized that these particles would have free RAFT end groups (trithiocarbonate and alkyne) available to act as anchoring points for further network formation with additional gold NPs. This colloid was centrifuged at 14 500 rpm for 6 min, and the supernatant was discarded to remove the unbound polymer. The colloid was then resuspended in a minimum amount of water to obtain 30 μL of intermediate hybrids of concentration 100 nM. An equimolar amount of centrifuged gold NPs (i.e., 30 μL, 100 nM) was added to the red intermediate hybrid colloid and mixed with a vortex mixer for 1 min. The colloid was then allowed to stand for 3 to 4 h. The process is shown in Scheme 1C. The dispersion was then diluted with ultrapure water to obtain a concentration of 6 nM and analyzed by UV−vis, DLS, and SERS. All of the samples are designated with the stock solution concentration.

Preparation of Raman-Barcoded Hybrid Nanoassemblies. Methylene blue (40 μL, 10^{-5} M) was added to the 6 nM hybrid nanoassemblies (Scheme 1D) to form barcoded nanoassemblies.

Characterization. *^{1}H NMR.* Proton nuclear magnetic resonance (^{1}H NMR) spectra was recorded using a Bruker 300 MHz spectrometer (Bruker BioSpin). Deuterated choloroform was used as the solvent.

GPC-MALLS. Molecular weights and molecular weight distributions were determined by size exclusion chromatography using a Waters HPLC system calibrated with polystyrene standards. Tetrahydrofuran (THF) was used as the eluent at a flow rate of 1.0 mL min^{-1}. A d*n*/d*c* value of 0.06 was used to calculate the M_w of the p(PEGMA) hyperbranched structures from the MALLS setup.

UV−Vis Spectroscopy. Ultraviolet−visible spectra were acquired using a Varian Cary 100 in the range of 400−900 cm^{-1} with a 1 cm path length cell with baseline correction.

Dynamic Light Scattering (DLS). DLS measurements were performed using a Malvern Zetasizer Nano Series running DTS software and a 4 mW He−Ne laser at 633 nm. Analysis was performed at an angle of 90° and a constant temperature of 25 °C. Dilute particle concentrations were used to ensure that multiple scattering and particle−particle interactions could be considered to be negligible.

Transmission Electron Microscopy. A JEOL 1010 transmission electron microscope (TEM) was used to study the NP morphologies on 200 mesh holey C-coated copper grids at 100 keV. As-prepared hybrid samples were diluted 100-fold and deposited on TEM grids so as to minimize the drying artifacts otherwise observed with higher concentrations (Figure S1 in Supporting Information). The median sizes were determined using iTEM software by measuring ∼110−120 individual assemblies per sample.

Raman Spectroscopy. SERS spectra were recorded with four accumulations in the spectral range of 200−2000 cm^{-1} with a Renishaw model InVia micro Raman spectrometer equipped with 785 nm excitation from a diode laser, a single diffraction grating, and an electrically cooled CCD detector. The laser power was 20 mW at the sample. Small-volume quartz cuvettes were used as sample holders.

Infrared Spectroscopy. Attenuated total reflectance-Fourier transform infrared (ATR-FTIR) spectra with 256 scans and a resolution of 4 cm^{-1} were obtained on a Nicolet Nexus 5700 FTIR spectrometer equipped with a Nicolet Smart Orbit single bounce containing a diamond ATR accessory (Thermo Electron Corp., Waltham, MA).

RESULTS AND DISCUSSION

Synthesis of Hyperbranched Polymers Using RAFT. Reversible addition−fragmentation chain-transfer (RAFT) polymerization is a controlled living radical polymerization technique with the benefit of using a large variety of monomers to yield low-polydispersity polymers while retaining the RAFT end groups.[54,55] We used a RAFT agent with a butyl trithiocarbonate group at one end (the z group) and an alkyne end-group (the R leaving group) as the other (as shown in Scheme 1B). The degree of branching in a hyperbranched polymer (HBP) system can be controlled by manipulating the polymer conversion, molar ratios of branching agent to RAFT agent, and monomer concentration.[56] At low branching, it generally forms a two-branch structure, whereas at higher degrees of branching it gels. Soluble HBPs with optimum branching were found to occur at higher conversions, 1:1 molar ratios of branching agent and RAFT agent with a monomer concentration of 1 mol L^{-1}. The number of branches was calculated on the basis of the M_n of the HBP, determined from GPC-MALLS and the M_n of a linear chain from ^{1}H NMR. A p(PEGMA) HBP with M_w = 100 kDa, number of branches N_b = 4 (i.e., four trithiocarbonate end groups and four alkyne end

dx.doi.org/10.1021/la304034b | *Langmuir* 2013, 29, 525−533

groups), and hydrodynamic diameter D_h = 8.5 ± 2 nm was synthesized and used in subsequent steps to mediate the formation of gold nanoassemblies. Similar data were obtained by Münnemann et al.[49] for their HBP structures.

Formation of an HBP-Mediated Hybrid Nanoassembly. Our strategy was to use a three-step process: (i) HBP-coated gold NPs, referred to as intermediate hybrids, were prepared, (ii) excess polymer and citrate were removed by centrifuging and concentrating the intermediate hybrids, and (iii) these intermediate hybrids were further added to equimolar gold NPs to form hybrid nanoassemblies.

When HBP was added to the gold colloid, because of the affinity of the trithiocarbonate[33] and alkyne[28−30] end groups for gold NPs, they bind to the gold NP surface, forming HBP-coated NPs. Because the HBPs have multiple end groups, it is hypothesized that the intermediate hybrids will have unbound trithiocarbonate and alkyne end groups on their surface, which are available to interact with additional gold NPs and thus act as the anchoring sites for the self-assembly of hybrid nanoassemblies. A concentration of 1 μM of HBP stock solution was added to a 2 nM gold NP colloid to prepare the intermediate hybrids with a final HBP concentration of ∼16.3 nM (sample designated as intermediate hybrid, 1 μM). Hence, the 1 μM intermediate hybrid has ∼8 HBPs/gold NP. (Refer to Table S1 and the Supporting Information for detailed calculations.) At this stage, λ_{SPR} had shifted slightly from 519 to 521 nm (Figure S2 in Supporting Information), the DLS mean diameter increased from 18 ± 3 to 33 ± 5 nm, and the zeta potential decreased from −50 to −14 mV. These results all indicate that HBP has self-assembled around the gold NP and also that aggregation has not occurred. The TEM image of a single NP as shown in Figure 2B confirms the presence of a polymer coating, seen as a halo around the gold NPs.

The unreacted HBP and excess citrate were removed from the intermediate hybrids by centrifugation. They were then resuspended in minimum water, increasing the concentration from 2 to 100 nM (designated as "X" NPs). Similarly, the excess citrate was removed from an equimolar citrate-stabilized gold colloid to concentrate it to 100 nM (designated as "Y" NPs). This step is crucial to the formation of hybrid nanoassemblies because otherwise the unreacted HBP and excess citrate might have a stabilization effect, hindering the possible interactions between the NPs. Concentrating the NPs also increases the possibility of the interaction of unbound RAFT end groups with other nearby NPs, thus facilitating the formation of nanoassemblies.

Finally, an equimolar amount (i.e., 1:1 [X]/[Y]) of the above centrifuged and concentrated citrate-stabilized gold NPs (Y NPs) was added to the centrifuged and concentrated intermediate hybrids (X NPs), allowing the available end groups of the intermediate hybrids to bind to the added gold NPs to form the hybrid gold nanoassemblies (sample designated as 1 μM hybrid nanoassemblies). The red color of well-dispersed citrate-stabilized gold NPs turned bluish on formation of the hybrid nanoassemblies. A prominent secondary UV−vis peak was observed at around 685 nm (Figure S2c in Supporting Information). The formation of the nanoassemblies was confirmed by TEM micrographs (Figure 1B) using very dilute samples (100-fold diluted) of the hybrid nanoassemblies.

To confirm that the assemblies observed by TEM were not due to coalescence during drying, we carried out some cryo-TEM studies and compared them to our normal TEM

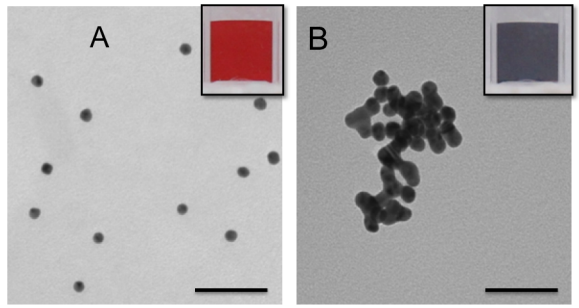

Figure 1. (A) TEM micrographs of citrate-stabilized gold NPs and (B) TEM of hybrid HBP−gold nanoassemblies. The color of each solution is shown in the inset. Scale bar = 100 nm.

micrographs. It was observed that at higher concentrations (as-prepared hybrid nanoassemblies) prominent drying artifacts were observed with normal TEM whereas on dilution (to 100 times that of the as-prepared hybrids) we could minimize drying artifacts and obtained similar results to that of cryo-TEM (Figure S1 in Supporting Information).

In contrast, no aggregation was observed for gold NPs when a nonionic linear methacrylate polymer, p(PEGMA), of $M_w \approx$ 30 kDa synthesized using RAFT polymerization and having only one binding end group (i.e., the thio end-group from the RAFT agent) was employed as the linker (Figure S3 in Supporting Information). A similar lack of aggregation of gold NPs stabilized by linear polymers with one dithioester group has been reported by Merican et al.[38] This emphasizes the importance of the polyvalent nature of the branched structures in the directed self-assembly process. The HBP-mediated hybrid nanoassemblies were visually observed to be stable (i.e., remained dispersed), and no further change in the color was observed for at least 2 to 3 months at room temperature.

Determination of HBP in the Hybrids. The presence of the polymer surrounding the gold NPs was confirmed by the halo observed in the TEM micrographs (Figure 2, as shown

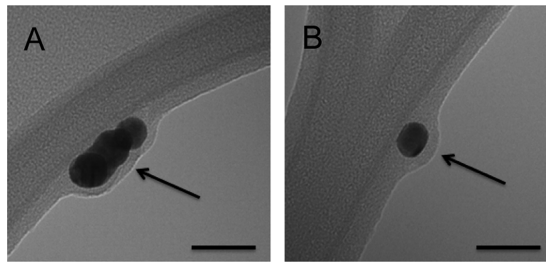

Figure 2. TEM micrographs of hybrid nanoassemblies protruding into the holes of a holey C-coated grid, confirming the presence of the polymer layer (as shown by arrows). Scale bar = 50 nm.

with an arrow) of hybrid nanoassemblies protruding into the holes of a holey C-coated grid. No halo was observed when imaging citrate-stabilized gold NPs (Figure S4 in Supporting Information).

In addition to the TEM images, the ATR-FTIR spectra (Figure 3) confirmed the presence of the HBP in the hybrid nanoassemblies. The peaks at 1726 (C═O stretch) and 2866, 1451, and 1379 cm^{-1} (CH bend and CH stretch) were present both in the HBP and hybrid nanoassemblies (Figure 3), confirming the presence of the polymer in the hybrid nanoassemblies.

dx.doi.org/10.1021/la304034b | Langmuir 2013, 29, 525−533

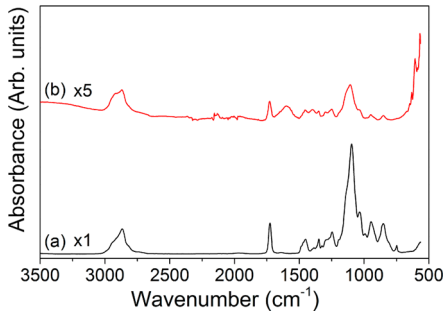

Figure 3. ATR-FTIR spectra of (a) HBP and (b) hybrid nanoassemblies showing the presence of polymer.

Influence of Polymer (HBP) Concentration on the Self-Assembly of Gold NPs. A certain degree of control over the size of the hybrid nanoassemblies and hot-spot density could be achieved by manipulating the polymer concentration (i.e., number of HBP particles per gold NP) when preparing the intermediate hybrids. The first set of data in evidence of this was the change in λ_{SPR} as a function of polymer concentration, which was observed by visible spectroscopy. The citrate-stabilized gold NPs have a λ_{SPR} at 519 nm because of the dipolar oscillation of electrons in the particles, which is expected for unaggregated particles. With an increase in polymer concentration, the λ_{SPR} was found to red shift with the appearance of a secondary peak at ~685 nm, which can be assigned to the multipolar oscillation of electrons, which is consistent with the aggregation of nanoparticles.[1,2,57] On further increasing the concentration of polymer, the secondary peak was not observed (Figure 4A). This effect was

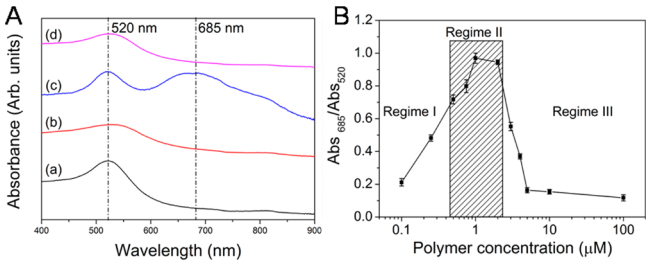

Figure 4. (A) UV−vis spectra of (a) citrate-stabilized gold NPs, (b) regime I hybrid nanoassemblies, (c) regime II hybrid nanoassemblies, and (d) regime III hybrid nanoassemblies. (B) Plot of the ratio of the absorbance at 685 nm to that at 520 nm vs the HBP concentration, showing the dependence of the assembly behavior on HBP concentration.

quantitatively studied by calculating the ratio of absorbance at 685 nm to that at 520 nm and its trend with increasing polymer concentration. As the polymer concentration was increased, it was observed that the ratio of Abs_{685}/Abs_{520} initially increased to a maximum for 1 μM concentration (≡ 16.3 nM in the intermediate hybrid) and then decreased (Figure 4B). These three different regions are respectively termed regimes I−III on the basis of the color of the hybrid solution and the observation of a secondary absorbance peak in the UV−vis spectrum (Figure 4).

To achieve a better understanding of the self-assembly behavior, the polymer concentration was related to the calculated surface coverage of the HBPs on the gold NPs for the intermediate hybrids (Table 1). (See Table S1 in Supporting Information for details of the calculation of surface coverage.)

Table 1. Polymer Concentrations and Surface Coverages of the Intermediate Hybrids

		intermediate hybrid NPs		
regime	polymer conc as added (μM)	polymer conc (nM)	no. of HBP per intermediate NP	calculated surface coverage %
I	<0.5	<8.19	<4	<12
II	0.5−2.0	8.19−32.78	4−17	12−47
III	>2.0	>32.78	>17	>47

With increasing polymer concentration in the formation of the intermediate hybrids (i.e., increasing HBP particle to gold NP ratio), more citrate ions get displaced by the HBP particles, thus increasing the surface coverage of the intermediate hybrids. The effect of polymer concentration on the nanoassemblies is depicted in the schematic shown in Figure 5A, along with their morphologies by TEM (Figure 5B), particle size distributions obtained from TEM (Figure 5C), and DLS hydrodynamic diameters (Figure 5D). At lower polymer concentrations in regime I, the hybrids remain red in color with minor red shifts and are composed predominantly of single NPs, dimers, and trimers and a TEM median size of 34 nm (Figure 5B). When the polymer concentration was increased (i.e., in regime II), there was a visible color change from red to bluish black, and a prominent secondary peak in the visible spectrum at around 685 nm was observed. Regime II nanoassemblies (Figure 5B) produced structured networks, both 3D assemblies and 1D linear nanochains, of size ranging from 50 to 120 nm formed from individual gold NPs of diameter ~17 nm. Interestingly, with further increases in polymer concentration only minimal shifts in the λ_{SPR} and small degrees of aggregation were observed by UV−vis and TEM, respectively, as compared to that of citrate-stabilized gold NPs.

These results can be explained within the framework of DLVO theory, which rationalizes the stability of colloids in solution and is summarized by eq 1

$$V_T = V_A + V_R + V_S \quad (1)$$

where the colloidal stability depends on the total potential energy function, V_T. V_S is the potential energy contribution from the solvent but is typically small. The most important factors are the contributions from attractive, V_A, and repulsive, V_R, forces where the balance of these opposing forces dictates the colloid stability. In DLVO theory, V_A varies with the inverse square of particle separation, and V_R is a more complex function that depends on the particle radius and zeta potential and decreases exponentially with particle separation.

For our system, the as-synthesized gold NPs are stabilized with citrate anions and have a zeta potential of −50 mV, where V_R outweighs V_A so that the probability of particle−particle collisions having sufficient kinetic energy to overcome the repulsive force is low. The attachment of HBP to the gold NP surface results in the displacement of citrate ions, resulting in a decrease in surface charge. Typically, the attachment of polymer is expected to provide steric stabilization of the colloids by forming a layer that negates the van der Waals attractive forces. However, in this case the HBPs are polyvalent, and it is expected that the intermediate hybrids will have free

dx.doi.org/10.1021/la304034b | Langmuir 2013, 29, 525−533

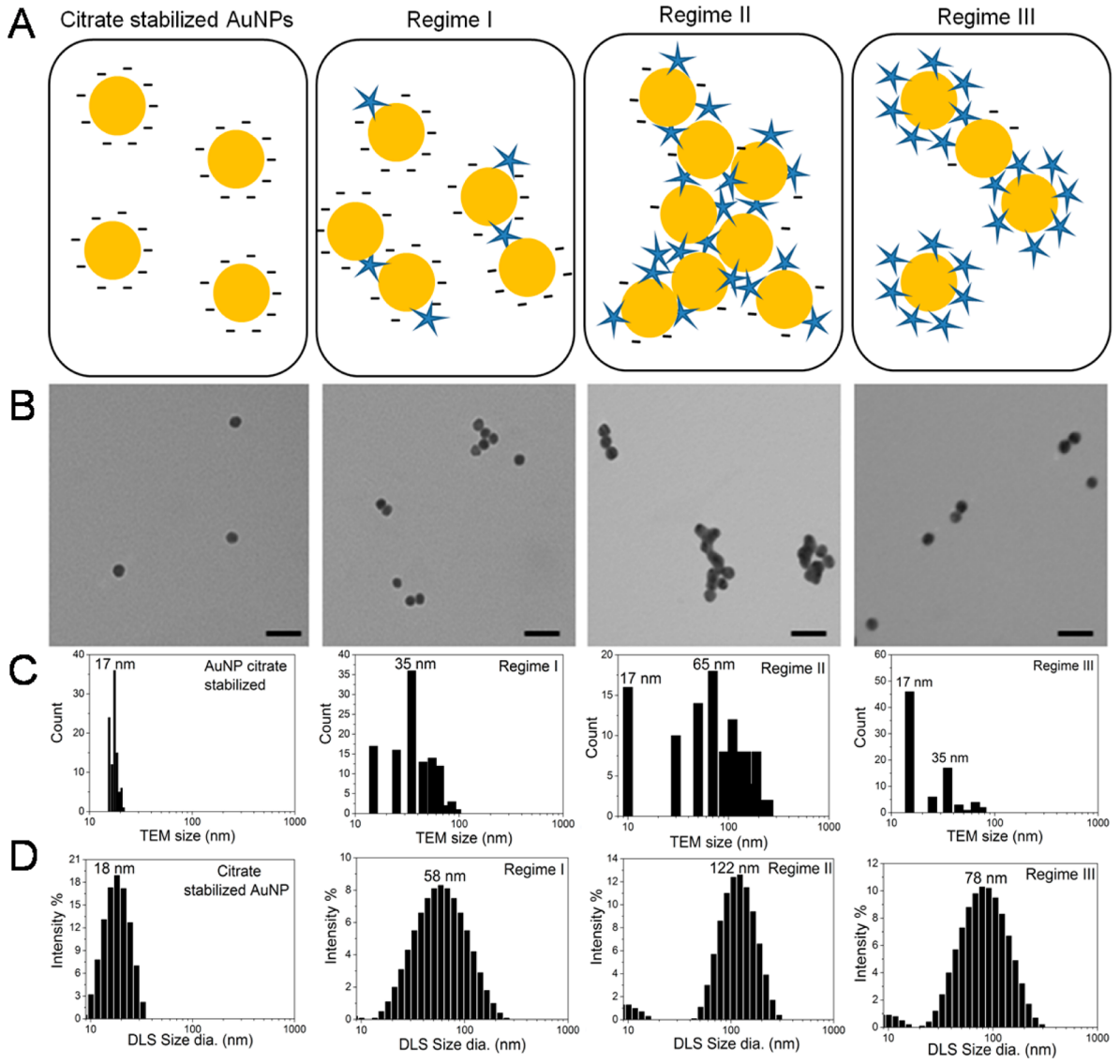

Figure 5. (Columns) Citrate stabilized gold NPs (AuNP's), regime I hybrid nanoassemblies, regime II hybrid nanoassemblies, and regime III hybrid nanoassemblies. (Rows) (A) Cartoon demonstrating possible morphologies of hybrid nanoassemblies in different regimes. (B) TEM micrographs (scale bar = 50 nm). (C) TEM median size and size distribution. (D) DLS hybrid hydrodynamic diameters and their distribution.

trithiocarbonate and alkyne end groups to facilitate coupling with the added NPs.

For regime I, the number of HBP particles per gold NP is less than 4, which corresponds to a surface coverage of less than 12% (Table 1 and section S5 in Supporting Information). The zeta potential of the particles falls within the range of −32 to −27 mV. In this scenario, the low coverage results in only a few sites on the NP that can couple to other NPs, so the probability of aggregation is low. In addition, the high negative surface charge is expected to promote stability.

For regime II, there are 4−17 HBP particles per gold NP, which corresponds to a surface coverage of 12−47%. In addition, the zeta potential dropped to between −27 and −13 mV. The drop in surface charge will decrease the repulsive force between the NPs, and with a relatively low coverage of polymer, there will be insufficient steric stabilization to screen the attractive van der Waals forces. In addition to this, the HBP coating is expected to have free trithiocarbonate and alkyne end groups that will bind to the added gold NPs. Because of contributions from both of these mechanisms, the attractive forces between the particles appear to be dominating and causing high levels of aggregation.

For regime III, the number of HBPs per NP is greater than 17, corresponding to a surface coverage of more than 47% so that most of the citrate ions are displaced and the zeta potential drops to −10 mV. In this case, the high coverage of HBP screens the attractive van der Waals forces between the NPs. Thus, both the intermediate hybrids and the additional citrate-stabilized gold NPs are each intrinsically stable because of the higher surface coverage of HBP (>47%) for the intermediate hybrids and the high zeta potential (−50 mV) of the citrate-stabilized NPs. However, when these NPs are brought close to each other, by centrifuging and concentrating the sample in the hybrid preparation step, some of the additional citrate-stabilized NPs bind to the free trithiocarbonate and alkyne end groups available on the surface of the intermediate hybrids, achieving a lower degree of aggregation compared to that in regime II. Hence, we mostly observe single NPs or dimers in regime III.

Raman-Barcoded Hybrid Nanoassemblies. A Raman tag molecule, methylene blue (MB), was added to the hybrid

dx.doi.org/10.1021/la304034b | *Langmuir* 2013, 29, 525−533

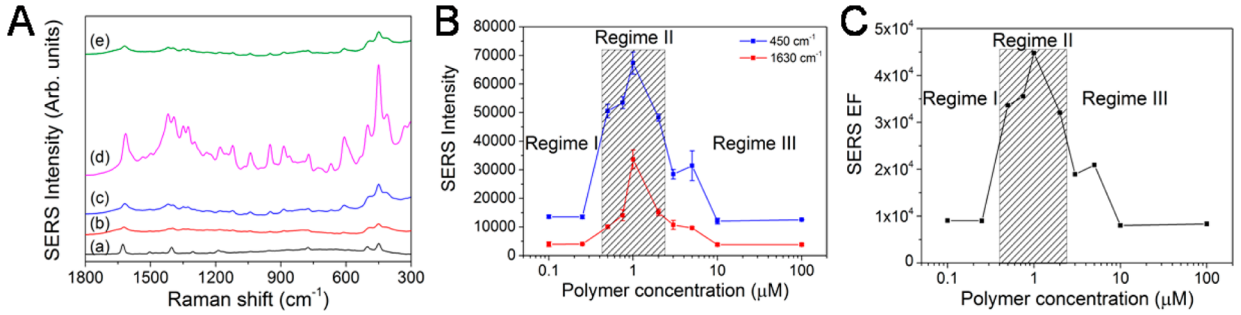

Figure 6. (A) (a) Raman spectrum of a 1 mM methylene blue (MB) solution. (b) SERS of MB-barcoded gold NPs. (c) SERS of the MB-barcoded regime I hybrid. (d) SERS of the MB-barcoded regime II hybrid. (e) SERS of the MB-barcoded regime III hybrid nanoassemblies. (B) Dependence of SERS intensity on the HBP concentration, showing the effect of regimes. (C) Effect of HBP concentration (regimes) on the SERS enhancement factor (EF).

nanoassemblies to obtain a final concentration of 3×10^{-7} M. These assemblies were then screened for their SERS enhancements in the solution state, keeping the gold NP and MB concentrations the same for all samples. The prominent peaks of MB at 450 and 1628 cm^{-1} were present in the SERS spectra of the hybrid nanoassemblies. Both regimes I and III show a SERS enhancement (Figure 6Ac,e) greater than that of the citrate-stabilized gold NPs (Figure 6Ab). The maximum enhancement was achieved with the larger nanoassemblies of regime II and was found to be 4 to 5 times that obtained for regime I and III hybrids (Figure 6B). Hence, it is justified to state that hybrid nanoassemblies enhance the SERS signal and thus may find application as Raman-barcoded assemblies. An enhancement factor (EF) in the range of $(1-4.5) \times 10^4$ was obtained for the hybrid nanoassemblies. (See Figure 6C and section S6 in Supporting Information for SERS EF calculation details.)

The average SERS intensity for both the major peaks of MB (Figure 6B) was found to increase from regime I to regime II and then decrease in regime III. The SERS intensity at a polymer concentration of 5 μM (second point in regime III) seems to increase with respect to the previous data point (3 μM concentration (first point in regime III); however, this may not be significant because the error in the SERS measurement of 5 μM is comparatively higher than that of other data points. The same trend also occurs in the SERS EF (Figure 6C) because the EF is calculated on the basis of the average SERS intensity. The highest EF of 4.5×10^4 was obtained with regime II nanoassemblies. This behavior is probably due to the fact that the larger nanoassemblies in regime II have a higher number of NPs in each nanoassembly and hence a higher density of hot spots, which increases the SERS signal and the EF. Although the EF obtained in these experiments is good, it should be noted that the nanoassemblies might not have reached their maximum potential because the Raman tag molecules were added after the formation of the hybrids. Consequently, every hot spot may not be accessible to the tags. If Raman tags were added earlier in the preparation method, it might increase the possibility of them reaching and occupying more hot spots within the nanoassembly and hence may improve the SERS enhancement. Further enhancements could be obtained with careful optimization of the NP shape, size, and hot-spot density of such hybrid nanoassemblies.

SERS Multiplexing Capability of Hybrid Nanoassemblies. Different Raman tags were employed in the study of the SERS response of the nanoassemblies. Figure 7 shows the SERS spectra for barcoded hybrid nanoassemblies with 2-quinolinethiol (2-QTH), indocyanine green, and adenine emphasizing that 2-QTH serves as a better tag having prominent peaks compared to the others. This provides the possibility of multiplexing (i.e., barcoding the nanoassemblies with different Raman tags), an essential tool required for biodiagnostic applications.

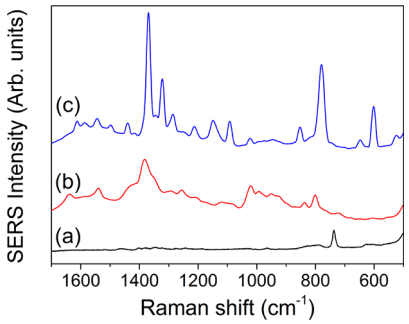

Figure 7. SERS spectra of barcoded regime II hybrid nanoassemblies with different Raman tags: (a) adenine, (b) indocyanine green, and (c) 2-quinolinethiol.

CONCLUSIONS

We have demonstrated a simple strategy to control the formation of gold NP assemblies. As a proof of concept, we have shown that hyperbranched polymer architectures with multiple anchoring end groups can be successfully employed to self-assemble gold NPs into hybrid nanoassemblies. In contrast, a linear polymer having only one anchoring end group does not form aggregated nanoassemblies, thus emphasizing the importance of the polyvalent nature of the branched structures in the linker-mediated self-assembly process. These hybrid nanoassemblies have sizes in the range of 20–120 nm. The effect of HBP concentration on the self-assembly process has been studied in detail, where the size of the hybrid nanoassemblies, (i.e., the self-assembly behavior of such systems) can be controlled to a certain extent by manipulating the polymer concentration and the surface coverage of the intermediate hybrids. Both low (<12%) and high (>47%) surface coverage results in smaller hybrid nanoassemblies, with a fewer number of NPs per assembly and a lower hot-spot density, giving rise to a moderate SERS enhancement ($\sim 1 \times 10^4$). With 12–47% HBP surface coverage, which we have termed regime II, larger nanoassemblies with a greater number of NPs per assembly and higher hot-spot densities were formed. These regime II Raman-barcoded hybrid nanoassemblies have a

dx.doi.org/10.1021/la304034b | Langmuir 2013, 29, 525–533

significantly better SERS enhancement that the other regime assemblies (~5-fold), achieving an enhancement factor (EF) of 4.5×10^4 (solution phase) with 3.0×10^{-7} M methylene blue. We have also demonstrated that these nanoassemblies can be barcoded with different Raman tag molecules, which would be beneficial for multiplexing in biodiagnostic applications. Such Raman-barcoded hyperbranched polymer-mediated gold NP assemblies with further optimization of the NP shape, size, and hot-spot density may find application as SERS diagnostic probes in nanomedicine.

■ ASSOCIATED CONTENT

Supporting Information

TEM and cryo-TEM micrograph comparison. UV−vis spectra comparison of gold NPs, intermediate hybrids, and hybrid nanoassemblies. TEM images of polymer-coated NPs in hybrid nanoassemblies. Surface-coverage calculation. SERS EF calculations. This material is available free of charge via the Internet at http://pubs.acs.org.

■ AUTHOR INFORMATION

Corresponding Author

*E-mail: p.fredericks@qut.edu.au.

Notes

The authors declare no competing financial interest.

■ ACKNOWLEDGMENTS

This research was supported under the Australian Research Council (ARC) Discovery Projects Scheme (project number DP1094205). I.B. and K.J.T. acknowledge the ARC for Future Fellowship funding (FT100100721 and FT110100284). This work was performed in part at the Queensland node of the Australian Microscopy and Microanalysis Research Facility (AMMRF) within the Centre of Microscopy and Microanalysis (CMM). We also acknowledge Dr. Craig Bell (AIBN, UQ) for providing us with the precursors for the RAFT agent. Thanks are also due to Dr. Llewellyn Rintoul for assistance in obtaining Raman spectra.

■ REFERENCES

(1) Jain, P. K.; El-Sayed, M. A. Plasmonic coupling in noble metal nanostructures. *Chem. Phys. Lett.* **2010**, *487*, 153−164.
(2) Jain, P. K.; Huang, W.; El-Sayed, M. A. On the universal scaling behavior of the distance decay of plasmon coupling in metal nanoparticle pairs: a plasmon ruler equation. *Nano Lett.* **2007**, *7*, 2080−2088.
(3) Hao, E.; Schatz, G. C. Electromagnetic fields around silver nanoparticles and dimers. *J. Chem. Phys.* **2004**, *120*, 357−366.
(4) Adleman, J. R.; Boyd, D. A.; Goodwin, D. G.; Psaltis, D. Heterogenous catalysis mediated by plasmon heating. *Nano Lett.* **2009**, *9*, 4417−4423.
(5) Austin, L. A.; Kang, B.; Yen, C.-W.; El-Sayed, M. A. Plasmonic imaging of human oral cancer cell communities during programmed cell death by nuclear-targeting silver nanoparticles. *J. Am. Chem. Soc.* **2011**, *133*, 17594−17597.
(6) Giljohann, D.; Seferos, D.; Daniel, W.; Massich, M.; Patel, P.; Mirkin, C. Gold nanoparticles for biology and medicine. *Angew. Chem., Int. Ed.* **2010**, *49*, 3280−3294.
(7) Alvarez-Puebla, R. A.; Liz-Marzán, L. M. SERS-based diagnosis and biodetection. *Small* **2010**, *6*, 604−610.
(8) De, M.; Ghosh, P. S.; Rotello, V. M. Applications of nanoparticles in biology. *Adv. Mater.* **2008**, *20*, 4225−4241.
(9) Alvarez-Puebla, R. A.; Liz-Marzán, L. M. Environmental applications of plasmon assisted Raman scattering. *Energy Environ. Sci.* **2010**, *3*, 1011−1017.
(10) Halvorson, R. A.; Vikesland, P. J. Surface-enhanced Raman spectroscopy (SERS) for environmental analyses. *Environ. Sci. Technol.* **2010**, *44*, 7749−7755.
(11) Bantz, K. C.; Meyer, A. F.; Wittenberg, N. J.; Im, H.; Kurtulus, O.; Lee, S. H.; Lindquist, N. C.; Oh, S.-H.; Haynes, C. L. Recent progress in SERS biosensing. *Phys. Chem. Chem. Phys.* **2011**, *13*, 11551−11567.
(12) Lin, X. M.; Cui, Y.; Xu, Y. H.; Ren, B.; Tian, Z. Q. Surface-enhanced Raman spectroscopy: substrate-related issues. *Anal. Bioanal. Chem.* **2009**, *394*, 1729−1745.
(13) Guerrini, L.; Graham, D. Molecularly-mediated assemblies of plasmonic nanoparticles for surface-enhanced Raman spectroscopy applications. *Chem. Soc. Rev.* **2012**, *41*, 7085−7107.
(14) Jin, R. Nanoparticle clusters light up in SERS. *Angew. Chem., Int. Ed.* **2010**, *49*, 2826−2829.
(15) Braun, G. B.; Lee, S. J.; Laurence, T.; Fera, N.; Fabris, L.; Bazan, G. C.; Moskovits, M.; Reich, N. O. Generalized approach to SERS-active nanomaterials via controlled nanoparticle linking, polymer encapsulation, and small-molecule infusion. *J. Phys. Chem. C* **2009**, *113*, 13622−13629.
(16) Brown, L. O.; Doorn, S. K. Optimization of the preparation of glass-coated, dye-tagged metal nanoparticles as SERS substrates. *Langmuir* **2008**, *24*, 2178−2185.
(17) Sanles-Sobrido, M.; Exner, W.; Rodríguez-Lorenzo, L.; Rodríguez-González, B.; Correa-Duarte, M. A.; Álvarez-Puebla, R. A.; Liz-Marzán, L. M. Design of SERS-encoded, submicron, hollow particles through confined growth of encapsulated metal nanoparticles. *J. Am. Chem. Soc.* **2009**, *131*, 2699−2705.
(18) Qian, X.; Peng, X. H.; Ansari, D. O.; Goen, Q. Y.; Chen, G. Z.; Shin, D. M.; Yang, L.; Young, A. N.; Wang, M. D.; Nie, S. *In vivo* tumor targeting and spectroscopic detection with surface-enhanced Raman nanoparticle tags. *Nat. Biotechnol.* **2008**, *26*, 83−90.
(19) Peer, D.; Karp, J. M.; Hong, S.; Farokhzad, O. C.; Margalit, R.; Langer, R. Nanocarriers as an emerging platform for cancer therapy. *Nat. Nanotechnol.* **2007**, *2*, 751−760.
(20) Yuan, F.; Dellian, M.; Fukumura, D.; Leunig, M.; Berk, D. A.; Torchilin, V. P.; Jain, R. K. Vascular permeability in a human tumor xenograft: molecular size dependence and cutoff size. *Cancer Res.* **1995**, *55*, 3752−3756.
(21) Romo-Herrera, J. M.; Alvarez-Puebla, R. A.; Liz-Marzán, L. M. Controlled assembly of plasmonic colloidal nanoparticle clusters. *Nanoscale* **2011**, *3*, 1304−1315.
(22) Alivisatos, A. P.; Johnsson, K. P.; Peng, X. G.; Wilson, T. E.; Loweth, C. J.; Bruchez, M. P.; Schultz, P. G. Organization of 'nanocrystal molecules' using DNA. *Nature* **1996**, *382*, 609−611.
(23) Loweth, J.; Caldwell, W. B.; Peng, X. G.; Alivisatos, A. P.; Schultz, P. G. DNA-based assemblies of gold nanocrystal. *Angew. Chem., Int. Ed.* **1999**, *38*, 1808−1812.
(24) Li, Z.; Zhu, Z.; Liu, W.; Zhou, Y.; Han, B.; Gao, Y.; Tang, Z. Reversible plasmonic circular dichroism of au nanorod and dna assemblies. *J. Am. Chem. Soc.* **2012**, *134*, 3322−3325.
(25) Hussain, I.; Wang, Z.; Cooper, A. I.; Brust, M. Formation of spherical nanostructures by the controlled aggregation of gold colloids. *Langmuir* **2006**, *22*, 2938−2941.
(26) Letsinger, R. L.; Elghanian, R.; Viswanadham, G.; Mirkin, C. A. Use of a steroid cyclic disulfide anchor in constructing gold nanoparticle-oligonucleotide conjugates. *Bioconjugate Chem.* **2000**, *11*, 289−291.
(27) Chen, J.; Jiang, J.; Gao, X.; Gong, J.; Shen, G.; Yu, R. Gold-aggregated, dye-embedded, polymer-protected nanoparticles (GDPNs): a new type of tags for detection with SERS. *Colloids Surf., A* **2007**, *294*, 80−85.
(28) Joo, S. W.; Kim, K. Adsorption of phenylacetylene on gold nanoparticle surfaces investigated by surface-enhanced Raman scattering. *J. Raman Spectrosc.* **2004**, *35*, 549−554.

(29) McDonagh, A. M.; Zareie, H. M.; Ford, M. J.; Barton, C. S.; Markovic, M. G.; Matisons, J. G. Ethynylbenzene monolayers on gold: a metal-molecule binding motif derived from a hydrocarbon. *J. Am. Chem. Soc.* **2007**, *129*, 3533−3538.
(30) Zhang, S.; L.Chandra, K.; B.Gorman, C. Self-assembled monolayers of terminal alkynes on gold. *J. Am. Chem. Soc.* **2007**, *129*, 4876−4877.
(31) Joo, S.-W.; Kim, W.-J.; Yoon, W. S.; Choi, I. S. Adsorption of 4,4′-biphenyl diisocyanide on gold nanoparticle surfaces investigated by surface-enhanced Raman scattering. *J. Raman Spectrosc.* **2003**, *34*, 271−275.
(32) Blakey, I.; Merican, Z.; Rintoul, L.; Chuang, Y. M.; Jack, K. S.; Micallef, A. S. Interactions of iodoperfluorobenzene compounds with gold nanoparticles. *Phys. Chem. Chem. Phys.* **2012**, *14*, 3604−3611.
(33) Duwez, A. S.; Guillet, P.; Colard, C.; Gohy, J. F.; Fustin, C. A. Dithioesters and trithiocarbonates as anchoring groups for the "grafting-to" approach. *Macromolecules* **2006**, *39*, 2729.
(34) Blakey, I.; Schiller, T. L.; Merican, Z.; Fredericks, P. M. Interactions of phenyldithioesters with gold nanoparticles (AuNPs): implications for AuNP functionalization and molecular barcoding of AuNP assemblies. *Langmuir* **2010**, *26*, 692−701.
(35) Boyer, C.; Whittaker, M. R.; Luzon, M.; Davis, T. P. Design and synthesis of dual thermoresponsive and antifouling hybrid polymer/gold nanoparticles. *Macromolecules* **2009**, *42*, 6917−6926.
(36) Corbierre, M. K.; Cameron, N. S.; Lennox, R. B. Polymer-stabilized gold nanoparticles with high grafting densities. *Langmuir* **2004**, *20*, 2867−2873.
(37) Luo, S.; Xu, J.; Zhang, Y.; Liu, S.; Wu, C. Double hydrophilic block copolymer monolayer protected hybrid gold nanoparticles and their shell cross-linking. *J. Phys. Chem. B* **2005**, *109*, 22159−22166.
(38) Merican, Z.; Schiller, T. L.; Hawker, C. J.; Fredericks, P. M.; Blakey, I. Self-assembly and encoding of polymer-stabilized gold nanoparticles with surface-enhanced Raman reporter molecules. *Langmuir* **2007**, *23*, 10539−10545.
(39) Jia, H.; Bai, X.; Li, N.; Yua, L.; Zheng, L. Siloxane surfactant induced self-assembly of gold nanoparticles and their application to SERS. *CrystEngComm* **2011**, *13*, 6179−6184.
(40) Toderas, F.; Baia, M.; Baia, L.; Astilean, S. Controlling gold nanoparticle assemblies for efficient surface-enhanced Raman scattering and localized surface plasmon resonance sensors. *Nanotechnology* **2007**, *18*, 255702.
(41) Lee, T.-C.; Scherman, O. A. Formation of dynamic aggregates in water by cucurbit[5]uril capped with gold nanoparticles. *Chem. Commun.* **2010**, *46*, 2438−2440.
(42) Polavarapu, L.; Xu, Q. H. Water-soluble conjugated polymer-induced self-assembly of gold nanoparticles and its application to SERS. *Langmuir* **2008**, *24*, 10608−10611.
(43) Boal, A. K.; Ilhan, F.; DeRouchey, J. E.; Thurn-Albrecht, T.; Russell, T. P.; Rotello, V. M. Self-assembly of nanoparticles into structured spherical and network aggregates. *Nature* **2000**, *404*, 746−748.
(44) Srivastava, S.; Frankamp, B. L.; Rotello, V. M. Controlled plasmon resonance of gold nanoparticles self-assembled with PAMAM dendrimers. *Chem. Mater.* **2005**, *17*, 487−490.
(45) Pan, B.; Gao, F.; Ao, L.; Tian, H.; He, R.; Cui, D. Controlled self-assembly of thiol-terminated poly(amidoamine) dendrimer and gold nanoparticles. *Colloids Surf., A* **2005**, *259*, 89−94.
(46) Maye, M. M.; Luo, J.; Lim, I. S.; Han, L.; Kariuki, N. N.; Rabinovich, D.; Liu, T.; Zhong, C. J. Size-controlled assembly of gold nanoparticles induced by a tridentate thioether ligand. *J. Am. Chem. Soc.* **2003**, *125*, 9906−9907.
(47) Yan, H.; Lim, S. I.; Zhang, L. C.; Gao, S. C.; Mott, D.; Le, Y.; Loukrakpam, R.; An, D. L.; Zhong, C. J. Rigid, conjugated and shaped arylethynes as mediators for the assembly of gold nanoparticles. *J. Mater. Chem.* **2011**, *21*, 1890−1901.
(48) Tan, J. H.; McMillan, N. A. J.; Payne, E.; Alexander, C.; Heath, F.; Whittaker, A. K.; Thurecht, K. J. Hyperbranched polymers as delivery vectors for oligonucleotides. *J. Polym. Sci., Polym. Chem.* **2012**, *50*, 2585−2595.
(49) Münnemann, K.; Kölzer, M.; Blakey, I.; Whittaker, A. K.; Thurecht, K. J. Hyperbranched polymers for molecular imaging: designing polymers for parahydrogen induced polarisation (PHIP). *Chem. Commun.* **2012**, *48*, 1583−1585.
(50) Thurecht, K. J.; Blakey, I.; Peng, H.; Squires, O.; Hsu, S.; Alexander, C.; Whittaker, A. K. Functional hyperbranched polymers: toward targeted in vivo ^{19}F magnetic resonance imaging using designed macromolecules. *J. Am. Chem. Soc.* **2010**, *132*, 5336−5337.
(51) Frens, G. Controlled nucleation for the regulation of the particle size in monodisperse gold suspensions. *Nature* **1973**, *241*, 20−22.
(52) Turkevich, J.; Stevenson, P. C.; Hillier, J. The formation of colloidal gold. *J. Phys. Chem.* **1953**, *57*, 670−673.
(53) Lai, J. T.; Filla, D.; Shea, R. Functional polymers from novel carboxyl-terminated trithiocarbonates as highly efficient RAFT agents. *Macromolecules* **2002**, *35*, 6754−6756.
(54) Moad, G.; Chong, Y. K.; Postma, A.; Rizzardo, E.; Thang, S. H. Advances in RAFT polymerization: the synthesis of polymers with defined end-groups. *Polymer* **2005**, *46*, 8458−8468.
(55) Perrier, S.; Takolpuckdee, P. Macromolecular design via reversible addition−fragmentation chain transfer (RAFT)/xanthates (MADIX) polymerization. *J. Polym. Sci., Polym. Chem.* **2005**, *43*, 5347−5393.
(56) Liu, B.; Kazlauciunas, A.; Guthrie, J. T.; Perrier, S. Influence of reaction parameters on the synthesis of hyperbranched polymers via reversible addition fragmentation chain transfer (RAFT) polymerization. *Polymer* **2005**, *46*, 6293−6299.
(57) Basu, S.; Ghosh, S. K.; Kundu, S.; Panigrahi, S.; Praharaj, S.; Pande, S.; Jana, S.; Pal, T. Biomolecule induced nanoparticle aggregation: effect of particle size on interparticle coupling. *J. Colloid Interface Sci.* **2007**, *313*, 724−734.